International Journal of Thermophysics, Vol. 24, No. 1, January 2003 (© 2003)

An Improved Transient Calorimetric Technique for Measuring the Total Hemispherical Emittance of Nonconducting Materials (Emittance Evaluation of Glass Sheets)

H. Masuda,[1] S. Sasaki,[2,3] H. Kou,[4] and H. Kiyohashi[5]

Received July 10, 2001

For measurements of the total hemispherical emittance ε_h of nonconducting materials, a problem of the thermal gradient produced in a sample specimen arises. An improved transient calorimetric technique to reduce the thermal gradient is proposed in this study. Glass sheets (borosilicate), semi-transparent for radiation, are selected as the nonconducting test material. The ε_h values of the glass sheets for various thicknesses are measured, and their results are presented as functions of thickness and temperature. The thermal gradients in the specimens are calculated by a three-dimensional analysis, and the corner effect due to them on the measured ε_h is estimated. It is shown that the proposed technique is useful for measuring the emittance ε_h of nonconducting materials.

KEY WORDS: calorimetric technique; glass sheet; nonconducting materials; total hemispherical emittance; thermal radiation.

1. INTRODUCTION

Direct measurements of the total emittance of solid materials are made radiometrically or calorimetrically [1, 2]; the total normal emittance, ε_n, (or the total directional emittance, ε) is evaluated by the radiometric

[1] Faculty of Technology, Tohoku Gakuin University, 1-13-1 Chuo, Tagajo 985-8537, Japan.
[2] Department of Mechanical Engineering, Ichinoseki National College of Technology, Hagisho-Aza-Takanashi, Ichinoseki 021-8511, Japan.
[3] To whom correspondence should be addressed. E-mail: seizi@ichinoseki.ac.jp
[4] Department of Information Mechanical Engineering, Daeble University, Chonnam 526-890, Korea.
[5] Department of Electrical Engineering, Ichinoseki National College of Technology, Hagisho-Aza-Takanashi, Ichinoseki 021-8511, Japan.

0195-928X/03/0100-0259/0 © 2003 Plenum Publishing Corporation

measurements, for example, as reported in Refs. 3–5, while the total hemispherical emittance, ε_h, is determined from calorimetric measurements. For the calorimetric measurements, there are three techniques usually applied, that is, (a) the pulse heating technique by resistive self-heating of a specimen [6], (b) the transient calorimetric technique (referred to hereafter as the TC technique) by heating a specimen with the use of a radio-frequency coil or furnace [7, 8], and (c) the steady-state calorimetric technique [9, 10].

As for the calorimetric measurements, the pulse-heating technique uses metal samples. This technique has been developed for measurements of multi-thermophysical properties including the emittance ε_h, mainly in the high temperature range (above 1000 K) [6], and many investigations, for example, Refs. 11–13, have been made. The TC technique has also been developed as a technique for measuring the emittance ε_h of metals [7, 8, 14], because a thermal gradient within a used metallic specimen rarely occurs during the cooling process and, hence, the temperature in the specimen is regarded as uniform. Further, the TC technique has been applied for simultaneous measurements of the emittance ε_h and the specific heat c of metals [15]. If the TC technique is applied to ε_h measurement of nonmetals (i.e., nonconducting materials), the technique must be modified. The steady-state calorimetric technique, using a heater in a prepared specimen, has not been easily used, because the thermal gradient within a specimen is too large. The present work aims at applying the TC technique to the ε_h measurement of nonconducting materials.

The total emittances of nonconducting materials can almost be measured with the radiometric technique. For this case, an important problem is the thermal gradients produced within specimens of nonconducting materials. To reduce the thermal gradients, some devices have been tried [3, 4], similar to those for spectral emittance measurements [16]. Recently, a study on the ε_h measurements on glass sheets was made by us to solve the above problem [17]. However, the measurements were carried out only in a narrow temperature range (about 350 to 450 K) because of the difficulty of fabricating specimens.

The TC technique is exceedingly convenient and useful for measuring the emittance ε_h of conducting materials. The objective of the present work is to develop the calorimetric technique to measure the emittance ε_h of nonconducting materials. An improved TC technique is proposed for the measurements in this work. Glass sheets are selected as the nonconducting materials for test measurements. The total emittance of the glass sheets has been previously investigated to some extent [3, 18], as it is interesting from a point of view of radiative heat transfer. The emittance ε_h of the sheets (borosilicate) are measured by the improved TC technique. Glasses are, in general, semi-transparent for some wavelength bands. Hence, the variation

of the measured ε_h with the thickness is experimentally verified. Thermal analysis is made for the glass sheet specimens used, and the thermal gradients in the specimens are calculated. The corner effect of the specimens on the measured ε_h due to the thermal gradients is evaluated.

2. APPLICATION OF THE TC TECHNIQUE TO NONCONDUCTING MATERIALS

2.1. Characteristics of the TC Technique

In the past, the TC technique has been applied for measurements of the emittance ε_h of metals. There are several investigations using sphere- [7], disk- [8] and wire-shaped [19, 20] specimens. When applying the TC technique, a specimen is placed in a vacuum chamber of an experimental apparatus, heated by, for example, a furnace to the desired temperature (the upper limit of temperature in the experiment), and then cooled to the ambient wall temperature (the lower limit of temperature) by radiation dissipation from the specimen. In Fig. 1, the cooling curve of the specimen, namely, the specimen temperature (T_s) versus time (t) curve is shown. During the cooling process (e.g., from 770 to 330 K in Ref. 19), the temperature decay is continuously recorded as shown in Fig. 1. The emittance ε_h of the specimen can be determined from the cooling rate dT_s/dt obtained from the curve for the cooling period. In the cooling process, if the specimen is metallic, the temperature within the specimen may be nearly uniform at any instant. For example, for the case of a spherical copper specimen with a diameter of 12 mm, the maximum temperature difference within the specimen, $\Delta T_{\max}$, was predicted to be 0.005 K at $T_s = 700$ K [7]. Axial temperature distributions in a wire specimen are shown in Fig. 2 as an example that the temperature differences are sensitive to position [20]. This figure indicates some numerical results analyzed for the situation that:

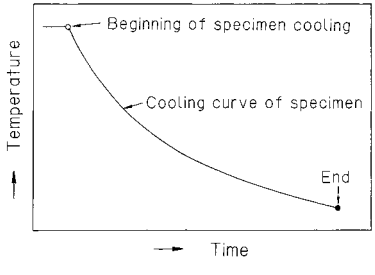

Fig. 1. Cooling curve by the usual TC technique.

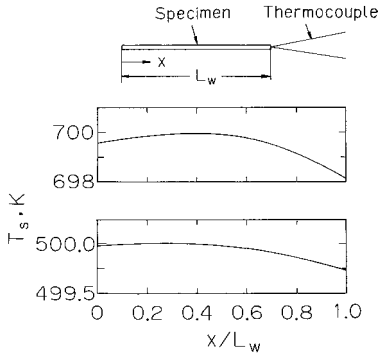

Fig. 2. Axial temperature distributions of the thin iron-wire specimen; 0.49 mm in diameter and 50 mm in length [20].

the iron-wire specimen with a diameter of 0.5 mm and a length of 50 mm is suspended by fine iron-constantan thermocouple leads (diameter 30 μm), and the cooling is begun from an initial temperature of 800 K inside the ambient wall maintained at liquid nitrogen temperature (77.4 K). From the figure, $\Delta T_{\max}$ along the wire axis is found to be very small (= 1.8 K) even for the iron wire having relatively low thermal conductivity. As seen from this example, the temperature differences in metallic specimens are very small even under such extreme conditions. The reason is that metallic materials have low emittance and high thermal conductivity. Therefore, the TC technique has been used as a technique suitable for measuring ε_h of conducting materials below 1000 K [7, 19, 21, 22]. The apparatus used is generally simple, compared with that for the radiometric measurement.

On the contrary, when the TC technique is applied for nonconducting materials, the temperature difference ΔT within the specimen may become large even if the specimen is small or thin, because of its relatively low thermal conductivity and high emittance. Results of thermal analysis for a glass specimen will be presented.

2.2. Temperature Distributions within Glass Specimen by Using the TC Technique

Thermal analysis is made for the rectangular solid specimen (Fig. 3) of borosilicate glass whose thermophysical properties are well known. In practice, the specimen may be suspended (see Fig. 6) by thermocouple leads attached at the center of surface B in Fig. 3 for measuring the specimen temperature. Hence, the leads must be carefully analyzed since the conduction heat loss Q_l through the leads has to be taken into account. However,

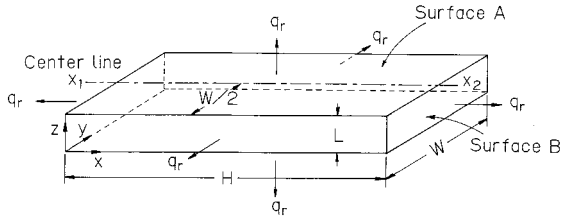

Fig. 3. Physical model for thermal analysis.

the quantity of Q_t is very small as described later, and Q_t can be neglected in this analysis. Consideration is given to the physical system for which the prepared specimen is placed in a vacuum chamber with blackbody walls of temperature T_∞, and allowed to cool by energy dissipation of the net radiative energy flux q_r from the specimen surface. For time t and Cartesian coordinates x, y, z as shown in Fig. 3, the transient heat-conduction equation for the temperature of the specimen, $T(x, y, z; t)$, can be expressed as

$$\frac{\partial T}{\partial t} = \alpha \left(\frac{\partial^2 T}{\partial x^2} + \frac{\partial^2 T}{\partial y^2} + \frac{\partial^2 T}{\partial z^2} \right) \tag{1}$$

where $\alpha[= \lambda/(c\rho)]$ is the thermal diffusivity of the specimen, and λ, c, and ρ are the thermal conductivity, specific heat, and density, respectively. Glass is the often-called radiative (i.e., absorbing, emitting, and scattering) medium, and, hence, radiative heat transfer arises within the specimen. If more rigorous analysis is needed, the energy equation must be derived for simultaneous conduction and radiation heat transfer. For this combined heat transfer, numerous investigations have been made for various media in the past [23]. In the present work, however, the radiation term in the energy equation is neglected, and Eq. (1) is used, because the thickness of the glass specimen used here is not so large and its optical thickness is very small as described in Section 4.2.

The initial condition for Eq. (1) is given, using the initial temperature T_i, as

$$T = T_i \qquad \text{for} \quad t = 0, \quad 0 \leqslant x \leqslant H, \quad 0 \leqslant y \leqslant W, \quad 0 \leqslant z \leqslant L \tag{2}$$

Specimen cooling is started after $t = 0$. The boundary condition on the specimen surface must be given. That may be derived as described in the following. The net radiative energy flux (energy per unit time and unit area) for an elemental area at an arbitrary position on the surface, e.g., the

position $(x, y, z = L)$ on surface A in Fig. 3, $q_{r,A}(x, y, z = L; t)$, is expressed as

$$q_{r,A} = \varepsilon_h^* \sigma T_A^{*4} - \alpha_h^* \sigma T_\infty^4 \tag{3}$$

where σ is the Stefan-Boltzmann constant, subscript A refers to surface A, and superscript * refers to the local position. The first term on the right-hand side of Eq. (1) accounts for the amount of energy emitted by the element, while the second term accounts for the energy which is incident on the element from the ambient black wall and the fraction of this energy which is absorbed by the element. The local total hemispherical emittance, ε_h^*, and the local total hemispherical absorptance, α_h^*, have to be used, taking into account the position on surface A, because the emittance and absorptance depend on temperature and the surface temperature of the specimen varies, especially in the corner parts (i.e., the corner effect). But yet, the properties ε_h^* and α_h^* may be substituted here, for convenience, by the hemispherical emittance ε_h $(T_{\text{A, cent}})$ and the hemispherical absorptance α_h $(T_{\text{A, cent}})$, respectively, at the center position of surface A, which are evaluated for the temperature at the center, $T_{\text{A, cent}}$. In the end, the boundary condition at the position $[x, y, z = L]$ on surface A and for time t can be expressed as

$$-\lambda \left.\frac{\partial T}{\partial z}\right|_{x, y, z = L; t} = \varepsilon_h(T_{\text{A, cent}})\, \sigma T_A^{*4} - \alpha_h(T_{\text{A, cent}})\, \sigma T_\infty^4 \tag{4}$$

For α_h in Eq. (4), Eq. (7), described later, can be applied if the ambient wall is black.

Equation (1) was solved with the conditions of Eqs. (2) and (4), and additionally with Eq. (7) for the specimen model having dimensions of $L = 3$ mm, $H = 50$ mm, and $W = 20$ mm and for some initial temperatures. For the values of λ, c, and ρ of borosilicate glass in the calculation, the data listed in Ref. 24 were used, and additionally the data in Ref. 16 were taken for the ε_h value. Typical results are shown in Fig. 4; the solid curves are the temperature profiles along the center line $[x_1 - x_2]$ on surface A in Fig. 3 for $T_i = 750$ K. As expected, the temperature decreases in the direction from the center to the corner. The temperature differences ΔT in the profiles are relatively small for small t after beginning the cooling ($\Delta T_{\max} = 5.5$ K at $t = 5$ s and for $T_i = 750$ K). But at $t = 50$ s, $\Delta T_{\max}$ is very large (about 16 K), and further, the temperature difference (or the thermal gradient) becomes larger with increasing time. From this observation, it is found that the cooling curve for a long time (e.g., $t > 10$ s for $T_i = 750$ K in this example) cannot be used to determine ε_h.

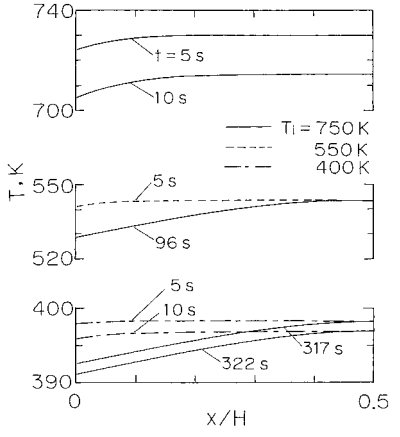

Fig. 4. Predicted temperatures at center line on the specimen surface: glass specimen model; $L = 3$ mm, $H = 50$ mm and $W = 20$ mm.

2.3. Improved TC Technique

With respect to the specimen of a nonconducting material, the increase in the thermal gradient cannot be avoided as mentioned above. However, for a short time after beginning the cooling, the thermal gradient is relatively small, and the cooling curve in this region may be used to determine the emittance. Some numerical results are presented below. In Fig. 4, the temperature profiles on the center line $[x_1 - x_2]$ for a short time t for $T_i = 550$ and 400 K are shown by dotted and dotted-dashed lines, respectively. Additionally, the profiles for $T_i = 750$ K, having the same temperatures at the center $x/H = 0.5$ as those of the above corresponding profiles, are shown in Fig. 4 for comparison. From the results, it is seen that, for example, $\Delta T_{\max}$ in the profile at $t = 5$ s and for $T_i = 550$ K is about 1.2 K, while that at $t = 96$ s and for $T_i = 750$ K is about 14 K; in turn, it is impossible to apply the usual TC technique such that the measurement is carried out over a wide temperature range, at least for a nonconducting specimen. However, if the wide temperature range is divided into many narrow sections, the TC technique can be applied to nonconducting specimens.

In each divided temperature range, the experiment by means of the TC technique, starting from T_i, is performed. Each temperature decay (cooling curve) is recorded as shown in Fig. 5; symbol ∘ indicates the beginning of cooling. As indicated in Fig. 4, the thermal gradient within the specimen just after the beginning is so small that the cooling curve for this time can

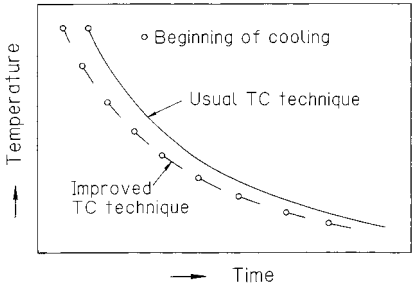

Fig. 5. Cooling curve for improved TC technique.

be used to determine ε_h. The cooling curve for $t \simeq 3$ to 8 s is suitable for this case. When the reference temperature (measured temperature) of the specimen is denoted by T_s, the cooling curve in the narrow temperature range may be expressed in the form [19],

$$T_s(t) = a \exp(-bt) \tag{5}$$

where a and b are constants. Using the cooling rate dT_s/dt obtained from Eq. (5), the emittance ε_h of the specimen can be determined from the following equation derived from the energy-balance equation for the specimen [21]:

$$\varepsilon_h(T_s) = \frac{-mc(T_s)\,\frac{dT_s}{dt}|_{T_s} + \sigma\alpha_h(T_s)\,FT_\infty^4 - Q_t}{\sigma FT_s^4} \tag{6}$$

where m, c, F, and α_h are, respectively, the mass, specific heat, surface area, and total hemispherical absorptance of the specimen, and Q_t is the conductive heat loss through the thermocouple leads suspending the specimen. In Eq. (6), for the value of c, there are published data available. For α_h, the appropriate value may be determined as follows: the ambient wall, namely, the inside wall of the vacuum chamber with temperature T_∞ is regarded as gray, since the wall is usually coated with black paint. In addition, if assuming that the spectral hemispherical emittance $\varepsilon_{h,\lambda}$ (subscript λ refers to wavelength λ) is a weak function of T, namely, $\varepsilon_{h,\lambda}(T_s) \simeq \varepsilon_{h,\lambda}(T_\infty)$, α_h is expressed as

$$\alpha_h(T_s) = \varepsilon_h(T_\infty) \tag{7}$$

In this study, Eq. (7) has been used for α_h in Eq. (6).

3. EXPERIMENTAL APPARATUS AND GLASS-SHEET SPECIMENS

The apparatus employed in previous work [17] was modified and used in the pressent work. The main parts of the apparatus are shown schematically in Fig. 6. The modified parts mainly involved the furnace heating a specimen and the gear moving the supporting rod of the furnace up-and-down.

As shown in Fig. 6, the specimen (3) was suspended by a thermocouple (4) at the center of the cooling bath (2) inside the vacuum chamber (1). At the centers of the end- and flat-surfaces of the specimen, pinholes, 0.5 mm in diameter, were cut with an ultrasonic machine, and the iron-constantan thermocouples of 50 μm diameter were inserted into them. The furnace core (8) inside the furnace (5) was made of copper, 35 mm inner diameter and 150 mm long, and had a narrow entrance part at the top. The core temperature was controlled with the electric sheath heater (9) wound outside the core. After the specimen had been heated to an initial temperature required in the furnace, the furnace was turned off and moved quickly together with its supporting rod outside the cooling bath by the gear (6). The vacuum in the chamber was better than $1–10^{-3}$ Pa, and the cooling

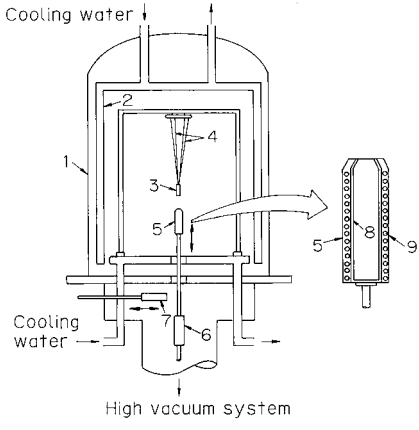

Fig. 6. Schematic of the experimental apparatus: (1) vacuum chamber; (2) cooling bath; (3) specimen; (4) thermocouple leads suspending specimen; (5) electric furnace for heating specimen; (6) gear for moving furnace; (7) radiation shield cover; (8) furnace core; (9) electric sheath heater.

Table I. Physical Description of Borosilicate Glass Specimens

Specimen number	L (mm)	H (mm)	W (mm)	m (g)
1	1.05	47.20	22.55	2.46
2	2.01	49.60	19.48	4.23
3	3.06	49.40	19.78	6.55
4	5.20	48.40	22.45	12.37

bath temperature was maintained at about 290 K by using a water bath. The experimental procedure was the same as that of Ref. 19.

Glasses, as nonconducting materials, are of great interest in the radiative properties, because of their semi-transparence. Various thermophysical properties of glasses, for example, fused silica, borosilicate, soda-lime, etc., have been measured and published. Nevertheless, there are few investigations on total emittance measurements of them [3, 4, 25, 26], although Gardon's papers [18, 27] are well known as theoretical studies. In the pressent work, four sheets of borosilicate glass of various thicknesses were selected as samples. The chemical components (%, by mass) were 80.9 S_iO_2, 12.7 B_2O_3, 4.0 Na_2O, 2.3 Al_2O_3, 0.04 K_2O, and 0.03 Fe_2O_3. Physical dimensions of the rectangular solid glass specimens used are given in Table I.

4. EXPERIMENTAL RESULTS AND DISCUSSION

4.1. Total Hemispherical Emittance ε_h of Glass Sheets

Typical results of the cooling curve are shown in Fig. 7. A part of the results is plotted in Fig. 8. From Fig. 8, these data are observed to follow a linear behavior from a least-squares analysis of the exponential function, as expressed in Eq. (5). The emittance ε_h of the glass specimens was obtained from Eqs. (5) and (6) with the temperature measured with the thermocouple attached at the center of the specimen's flat surface. For the evaluation of dT_s/dt, data for the cooling curve at $t = 4$ to 6 s were used. The higher the temperature and the thinner the specimen, the greater the value of dT_s/dt becomes. Calculations of the heat loss Q_t were made by the method used in Ref. 19, using the ε_h data of iron and constantan reported in Refs. 20 and 28, respectively. The ratio of Q_t to the total power loss of the specimen [i.e., the first term on the right-hand side of Eq. (6)] was less than 0.6%.

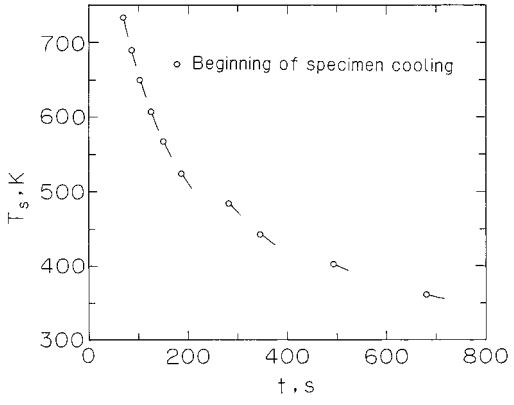

Fig. 7. Cooling curves of temperature versus time; Specimen 3.

The ε_h values of all the specimens, thus obtained, are shown in Fig. 9 as a function of T. Gardon's theoretical values [18] are also plotted in Fig. 9 for comparison; these values were obtained by using the spectral volume emissive power j_λ corresponding to the spectral volumetric coefficient J_λ in Sparrow and Cess [29]. It is evident from Fig. 9 that the emittance ε_h of the glass sheets decreases as the temperature increases. This is not surprising; solid materials have, in general, a characteristic that the total emitted energy (at all wavelengths) increases with increasing temperature and the peak spectral emissive power shifts toward a shorter wavelength as the temperature increases. In addition, glasses have another characteristic that their absorption coefficient κ is markedly low stepwise in the shorter wavelength region below about 2.7 μm [18, 30]. As a result of this behavior, the emittance ε_h of the glass sheets varies with temperature as shown in Fig. 9. Gardon's values (window glass, thickness $L = 2.0$ mm)

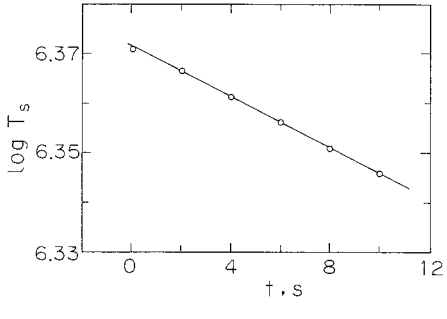

Fig. 8. Expression of the cooling curve as an exponential function; Specimen 3.

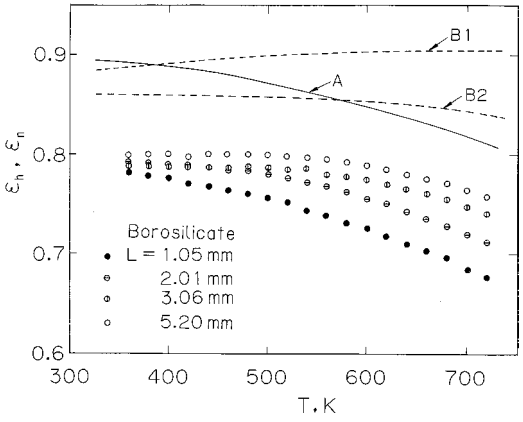

Fig. 9. Comparison of total emittance results for glass sheets: •, ⊕, ⊙ and ○, present work, ε_h of borosilicate glass, Specimens 1, 2, 3 and 4, respectively; line A, Gardon [18], theoretical, ε_h of window glass, $L = 2$ mm; lines B1 and B2, Olson and Morris [3], ε_n of borosilicate glass, $L = 4.76$ mm, and Pyrex 7740, $L = 12.7$ mm, respectively.

are larger than the present experimental values (borosilicate, $L \simeq 2.0$ mm) by 11 to 14%.

There are few data available for the total emittance of glass sheets. The results of Olson and Morris [3], obtained for borosilicate glass ($L = 4.76$ mm) and Pyrex glass 7740 ($L = 12.7$ mm) by the radiometric measurement technique, are shown in Fig. 9 as smooth curves. These data are for the emittance ε_n. For nonconducting materials, the emittance ε_n has generally been known to be higher than the emittance ε_h of the same material [31]. For the same reason, the ε_n data for borosilicate glass are likely higher than ε_h values for Specimen 4 with $L = 5.2$ mm (about 20%).

The ε_h values of semi-transparent solid materials vary with their thickness or optical thickness ($= \kappa L$), similar to those of radiative gas media [18, 30]. The ε_h variation of the borosilicate glass sheets with the thickness L is shown in Figs. 9 and 10. This property agrees in trend with the theoretical results for window glass sheets of Gardon [18]. The variation with the thickness is caused by the accumulation of radiative energy emitted from the volume elements within the glass specimen having a thickness L and by the transmission of the energy from within to outside the specimen. It is seen from Fig. 10 that the ε_h variation with the thickness is great in the thickness range of less than $L \simeq 5$ mm. Olson and Morris [3]

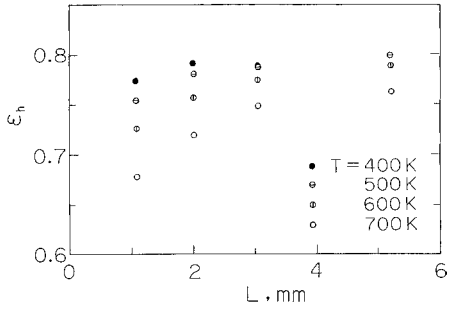

Fig. 10. Variation of total hemispherical emittance with sheet thickness.

measured the emittance ε_n of a number of glass sheets with a thickness larger than $L = 4.76$ mm for various glasses. For this thickness range, the ε_h variation appears very small, as seen from their ε_n results. From Fig. 10, additionally it is considered that the emittance ε_h near the corners (i.e., the edges) of the specimen is much lower than that at the central part, that is, the ε_h value is non-uniform over the specimen surface. However, the effect of this lower ε_h on the measured ε_h obtained from Eq. (6) is presumed to be slight, since the area of the lower ε_h is very small.

4.2. Temperature Distributions in Specimens and the Related Corner Effect on ε_h

The temperature distributions within the specimens are calculated again from Eq. (1). Before solving the equation, the validity of neglecting the radiation term to be involved in the heat-conduction equation, Eq. (1), will be discussed. In combined conduction and radiation heat transfer, the influence of radiation on the heat transfer strongly depends on the magnitude of the participating medium's optical thickness τ_0 ($=\kappa L$, dimensionless) [23]. Numerical solutions of the combined heat transfer in a one-dimensional planar system were obtained by Viskanta [31]. From the result it is found that the influence of the radiation on the temperature distributions is very slight; if τ_0 of the system is sufficiently small, in turn, the system is optically thin ($\tau_0 \ll 1$), and the parameter N [$=\lambda\kappa/(4\sigma T_s^3)$ where T_s is the reference temperature of the system.] which shows that the ratio of energy transfer by conduction to that by radiation is somewhat large. In the present work, for the borosilicate glass with $L = 5.2$ mm (the maximum in the pressent work) and under the conditions of $\kappa = 0.1\ \mathrm{cm}^{-1}$ [17], $\lambda = 1.6\ \mathrm{W \cdot m^{-1} \cdot K^{-1}}$ [24] and $T_s = 700$ K.

$$\tau_0 = 0.052, \qquad \text{and} \qquad N = 0.2 \tag{8}$$

From Ref. 31 and Eq. (8), it is apparent that the τ_0 values are so small that the radiation transfer within the specimen hardly affects the temperature distribution obtained by the present analysis.

Solutions of the specimen temperature for the two specimen models ($L = 1$ and 5 mm) were obtained, using Eqs. (1), (2), and (4). Here the present experimental results, as a function of the thickness (see Fig. 10), were used for ε_h, while the data of Ref. 24 were used for the other properties (c, λ, and ρ). The computed results are shown in Figs. 11 and 12. The solid curves in the figures represent the temperature distributions on the center lines of the specimen model which is illustrated in Fig. 11a; for example, the symbol a indicates the temperature on the center line $[x_1 - x_2]$ parallel to the x axis. All the results shown in Figs. 11 and 12 are those at 5 s after the specimen cooling begins (i.e., $t = 5$ s). From the figures, it is seen that the specimen temperature is considerably lower near the edges in the circumferential regions near the corners ($0 \leqslant x/H = y/W \sim 0.2$), compared with the central regions, but the magnitudes of the temperature drops in the center lines are not so large. The maximum temperature drops in the center lines are less than 6 K even for $T_i = 750$ K and less than 2.5 K for $T_i = 550$ K for specimen thicknesses of $L = 1$ and 5 mm. The temperature variation in the z-direction is also not so large; for example, the maximum temperature differences on the specimen tip surfaces for $T_i = 750$ K are less than 1.5 K for $L = 1$ mm and 3.5 K for $L = 5$ mm.

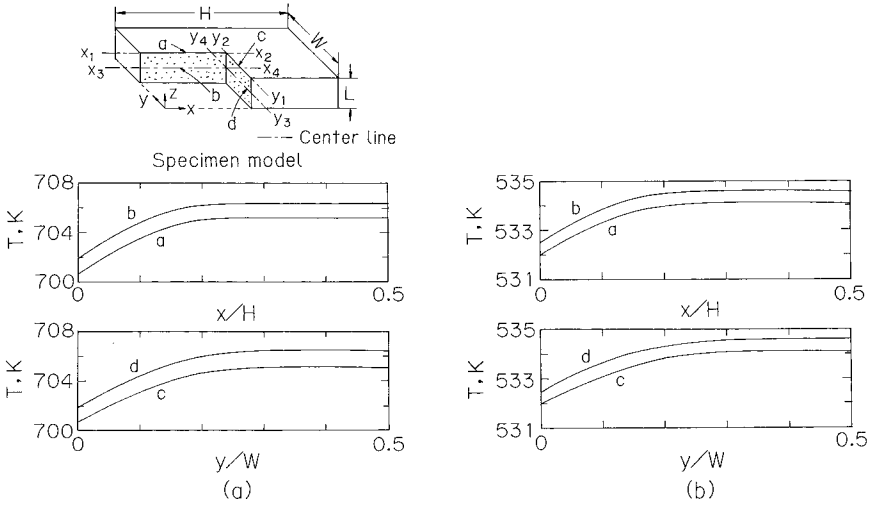

Fig. 11. Temperature distributions for the borosilicate specimen model of $L = 1$ mm, $H = 50$ mm, and $W = 20$ mm, and $t = 5$ s: (a) $T_i = 750$ K; (b) $T_i = 550$ K.

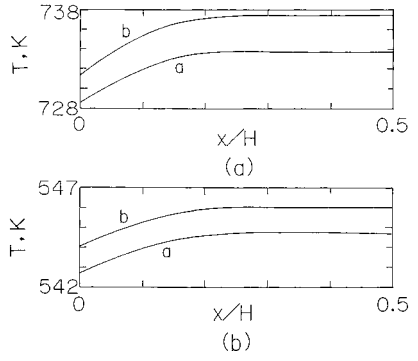

Fig. 12. Temperature distributions for the borosilicate specimen model of $L = 5$ mm, $H = 50$ mm, and $W = 20$ mm, and $t = 5$ s: (a) $T_i = 750$ K; (b) $T_i = 550$ K.

The error involved in the measured ε_h, caused by the temperature distribution (i.e., the thermal gradient) in the specimen, is considered to be relatively large. Therefore, the error should be estimated, although it is difficult to obtain its value accurately. The error analysis is described in the Appendix. As a result, the error in the present work was estimated to be 2.9% for Specimen 4 and $T_s \simeq 720$ K.

5. CONCLUSIONS

An improved TC technique for measuring the total hemispherical emittance ε_h of nonconducting materials is proposed. Semi-transparent (borosilicate) glass sheets were selected as the test materials, and ε_h values of the sheets for different thicknesses were measured. The emittance ε_h of grass sheets was expressed as functions of temperature and thickness. It was found that the ε_h values vary significantly with the thickness in the range of less than 5 mm. The thermal gradients within the specimens, produced in the cooling process, were calculated, and the effect of them on the measured ε_h was also discussed.

APPENDIX: ESTIMATE OF UNCERTAINTY CAUSED BY THE THERMAL GRADIENTS

If there is a thermal gradient in the specimen, the energy-balance equation for the specimen at an arbitrary time can be expressed as

$$-mc(T_m)\frac{dT_m}{dt} = \sigma \int_F \varepsilon_h(T_{sf})\, T_{sf}^4\, dF - \sigma \varepsilon_h(T_\infty)\, F T_\infty^4 + Q_t \tag{9}$$

where T_m is the volumetric mean temperature and T_{sf} is the local surface temperature $[= T_{sf}\ (x, y, z; t)]$ of the specimen. The value dT_m/dt may be approximated by the data at $T_s = T_m$ in the $\mathrm{d}T_s/\mathrm{d}t$ versus T_s curve for the specimen (omitted here), i.e.,

$$\frac{dT_m}{dt} \simeq \left.\frac{dT_s}{dt}\right|_{T_m} \tag{10}$$

Furthermore, since ε_h is a weak function of T, $\varepsilon_h(T_{sf})$ in Eq. (9) can be considered for the small temperature difference between T_{sf} and $T_{sf,m}$ (= the mean surface temperature) as

$$\varepsilon_h(T_{sf}) \simeq \varepsilon_h(T_{sf,m}) \tag{11}$$

By using these relations, $\varepsilon_h\ (T_{sf})$ in Eq. (9) can be expressed as

$$\varepsilon_h(T_{sf,m}) = \frac{-mc(T_m)\left.\frac{dt_s}{dt}\right|_{T_m} + \sigma\varepsilon_h(T_\infty)\, FT_\infty^4 - Q_t}{\sigma \int_F T_{sf}^4\, dF} \tag{12}$$

This value of $\varepsilon_h\ (T_{sf,m})$ obtained from Eq. (12) may be assumed as the real value of ε_h, $\varepsilon_{h,\mathrm{real}}$, and then this value is used for the estimate of the uncertainty in the measured ε_h, $\varepsilon_{h,\mathrm{mea}}$, obtained from Eq. (6). For T_{sf} in Eq. (12), the numerical solutions of Eq. (1) are applied.

The error in $\varepsilon_{h,\mathrm{mea}}$, caused by the thermal gradient, is given as

$$\left[\frac{\Delta\varepsilon_h}{\varepsilon_h}\right]_T = \frac{\varepsilon_{h,\mathrm{mea}} - \varepsilon_{h,\mathrm{real}}}{\varepsilon_{h,\mathrm{real}}} \tag{13}$$

The error $[\Delta\varepsilon_h\ /\ \varepsilon_h]_T$ becomes larger as the temperature T_s increases and the thickness L becomes larger.

NOMENCLATURE

c:	Specific heat
F:	Surface area
H, L, W:	Height, thickness, and width of specimen (Fig. 3)
m:	Mass
N:	Dimensionless parameter $[= \lambda\kappa/(4\sigma T_s^3)]$
Q_t:	Conduction heat loss through thermocouple leads
q_r:	Radiative energy flux
T:	Temperature
T_i:	Initial temperature
T_s:	Specimen temperature

T_∞:	Ambient wall temperature
t:	Time
x, y, z:	Coordinates in Cartesian system
α:	Thermal diffusivity
α_h:	Total hemispherical absorptance
ΔT:	Temperature difference between positions in specimen
ε_h:	Total hemispherical emittance
ε_n:	Total normal emittance
κ:	Absorption coefficient
λ:	Thermal conductivity
ρ:	Density
σ:	Stefan-Boltzmann constant
τ_0:	Optical thickness ($= \kappa L$)
Superscript	
*:	Local
Subscripts	
A:	Surface A
λ:	Wavelength λ

REFERENCES

1. J. C. Richmond, *Compendium of Thermophysical Property Measurement Methods*, Vol. 1, Survey of Measurement Techniques, K. D. Maglić, A. Cezairliyan, and V. E. Peletsky, eds. (Plenum Press, New York, 1984), Chap. 19, pp. 709–768.
2. T. Makino, *Progress in Heat Transfer*, New Series, Vol. 2, Japan Society Mechanical Engineers, ed. (Yokendo, Tokyo, 1996), pp. 169–250 (in Japanese).
3. O. H. Olson and J. C. Morris, *WADC Technical Report 56-222* (1960), Pt. 3, pp. 1–96.
4. W. A. Clayton, *Measurement of Thermal Radiation Properties of Solids*, J. C. Richmond, ed., NASA SP-31 (U.S. Government Printing Office, Washington, 1963), pp. 445–460.
5. T. Makino, M. Uchiyama, and B. D. Brajuskovic, *Jap. J. Thermophys. Prop., Netsu Bussei* **6**:8 (1992) (in Japanese).
6. A. Cezairliyan, M. S. Morse, H. A. Berman, and C. W. Beckett, *J. Res. Natl. Bur. Stand. (U.S.)* **74A**:65 (1970).
7. K. G. Ramanathan and S. H. Yen, *J. Opt. Soc. Am.* **67**:32 (1977).
8. H. Masuda and M. Higano, *J. Opt. Soc. Am. A* **2**:1877 (1985).
9. G. Best, *J. Opt. Soc. Am.* **36**:1009 (1949).
10. H. Masuda and M. Higano, *Trans. Jap. Soc. Mech. Eng. B* **50**:3051 (1984) [in Japanese].
11. R. E. Tayler, *High Temp.-High Press.* **13**:9 (1981).
12. I. Takahashi, A. Sugawara, and H. Mifune, *Heat Transfer Jap. Res.* **17**:29 (1988).
13. T. Matsumoto and A. Cezairliyan, *Int. J. Thermophys.* **18**:1539 (1997).
14. E. A. Estalote and K. G. Ramanathan, *J. Opt. Soc. Am.* **67**:39 (1977).
15. S. Sasaki, H. Masuda, M. Higano, and N. Hishinuma, *Int. J. Thermophys.* **15**:547 (1994).
16. H. O. McMahon, *J. Am. Ceram. Soc.* **34**:91 (1951).
17. S. Sasaki, H. Kiyohashi, H. Kou, and H. Masuda, *Proc. 3rd KSME-JSME Thermal Engineering Conf.*, Kyongju, Korea (1996), Vol. 3, pp. 333–338.
18. R. Gardon, *J. Am. Ceram. Soc.* **39**:278 (1956).

19. H. Masuda and M. Higano, *Trans. ASME, J. Heat Transfer* **110**:166 (1988).
20. H. Masuda and M. Higano, *Trans. Jap. Soc. Mech. Eng. B* **53**:573 (1987) [in Japanese].
21. R. Smally and A. J. Sievers, *J. Opt. Soc. Am.* **68**:1516 (1978).
22. S. X. Cheng, *Exp. Thermal and Fluid Sci.* **2**:165 (1989).
23. R. Viskanta, *Proc. 7th Int. Heat Trans. Conf.*, Washington (1982), Vol. 1, pp. 103–121.
24. *JSME Heat Transfer Handbook*, Japan Society Mechanical Engineers, ed. (Maruzen, Tokyo, 1993), p. 374 [in Japanese].
25. Y. S. Touloukian and D. P. DeWitt, eds., *TPRC Data Ser., Thermophysical Properties of Matter*, Vol. 8, *Thermal Radiative Properties* (IFI/Plenum, New York, 1972), pp. 1521–1650.
26. A. Ohnishi, T. Onoda, S. Yamamoto, S. Sanbe, and Y. Morita, *Trans. Inst. Elect. Eng. Jap.* **115-A**:471 (1995) [in Japanese].
27. R. Gardon, *Radiative Transfer from Solid Materials*, H. Blau and E. H. Fisher, eds. (Macmillan, New York, 1962), pp. 8–23.
28. H. Masuda, S. Sasaki, and M. Higano, *Exp. Thermal and Fluid Sci.* **4**:218 (1991).
29. E. M. Sparrow and R. D. Cess, *Radiation Heat Transfer*, Augmented Ed. (Hemisphere, New York, 1978), p. 18.
30. R. Siegel and J. R. Howell, *Thermal Radiation Heat Transfer*, 3rd edn. (Hemisphere, Washington, 1992), pp. 172–174, 631–642.
31. R. Viskanta and R. J. Grosh, *Trans. ASME, J. Heat Transfer* **84**:63 (1962).